

# The Free Electron Maser in Pulsar Magnetospheres

R. Schopper<sup>1,4</sup>, H. Ruhl<sup>2</sup>, T.A. Kunzl<sup>3</sup> and H. Lesch<sup>4</sup>

<sup>1</sup> Max-Planck-Institut für extraterrestrische Physik, Giessenbachstraße, 85740 Garching, Germany

<sup>2</sup> General Atomics, San Diego, CA, USA

<sup>3</sup> Max Planck Institut für Quantenoptik, Garching, Germany

<sup>4</sup> Universitäts-Sternwarte München, Scheinerstraße 1, 81679 München, Germany, Centre for Interdisciplinary Plasma Science

**Abstract.** We present the numerical simulations of coherent inverse Compton scattering (CICS) in a highly magnetized plasma process by means of a full three dimensional particle in cell code (PIC), which is mass and energy conservative. We used the parameters of a pulsar magnetosphere where CICS is one of the most promising models for the generation of the observed highly coherent radio emission. First we show details of the onset and time evolution of strong Langmuir turbulence driven by a relativistic electron beam penetrating a strongly magnetized background plasma. The Langmuir turbulence acts as self-generated wiggler fields which bunch the beam electrons thereby inducing strong coherent emission of the bunches at frequency  $\gamma^2$  times the plasma frequency. The emitted power is about 10 GW in a few nanoseconds. This radiation is interpreted in terms of inverse Compton scattering on nonlinear density fluctuations. CICS is the longitudinal version of a laboratory free electron laser and is applicable in strongly magnetized plasmas like pulsars.

## 1. Introduction

A strong source for coherent radiation in laboratory is the free electron laser (FEL) (O’Shea and Freund 2001). Its principle is the interaction of a relativistic electron beam (REB) and a magnetic wiggler system. The beam of high energy electrons with energy  $\gamma m_e c^2$  passes between permanent magnets of alternating polarity and periodicity  $\lambda_W$ . The energy of the REB is efficiently converted by electron bunching. In the observer’s frame the bunches emit the relativistically Doppler-shifted wavelength  $\lambda = \lambda_W / \gamma^2$ . A comparable effect can be driven by a REB penetrating a strongly magnetized plasma. In phase space such a configuration corresponds to a two-stream-instability. In the plasma version the free energy of the emitted radiation is supplied by the REB, as it is in the case of the FEL, but the positive gradient of the momentum distribution function  $df/dp > 0$  is the source of the instability which excites strong density fluctuations. In a strongly magnetized plasma such density oscillations are predominately longitudinal Langmuir waves which grow

to nonlinear amplitudes (Benford and Weatherall 1991), (Kato et al. 1983), (Weatherall 1988). The interaction of the REB with the electrostatic fluctuations of the Langmuir waves results in very strong coherent electromagnetic waves (Kato et al. 1983), (Levron et al. 1987). In the rest frame of the beam electrons, they experience the Doppler shifted electrostatic wave moving towards them. The nonlinear waves force the REB to wiggle and to emit dipole radiation of the same frequency as the waves. In the laboratory frame this Hertz’ dipole radiation is again Doppler boosted and strongly beamed in forward direction due to the relativistic lighthouse effect. This interaction can be viewed as coherent inverse Compton scattering (CICS) off Langmuir waves (Benford and Weatherall 1991). Coherence occurs due to the bunch structure of the beam which means a phase coupled electrostatic field and density modulation.

## 2. Computational Details

Since CICS has been discussed to be promising candidate for the origin of the extremely coherent radio emission from pulsars (Kunzl et al. 1998), (Melrose and Gedalin 1999), (Melrose 2000), we use the physical parameters of a pulsar magnetosphere as an instructive application. Radio observations indicate that at about 500 km from the strongly magnetized neutron star the coherent pulsed radio emission is produced. The coherence is proved by pulse substructures on time scales down to a few tens of nanoseconds with increasing flux densities (Rickett 1995). In these regions of a pulsar magnetosphere typical values are: background electron density  $n_e = 10^{12} \text{ m}^{-3}$ , beam electron density equal to the plasma density  $n_b = 10^{12} \text{ m}^{-3}$ , beam electron Lorentz factor  $\gamma = \sqrt{5}$  ( $\gamma\beta = 2$ ) and an extremely strong background magnetic field  $B$  of about 1000 T. Especially the strong guiding field is important for the efficiency of the CICS-process. It reduces the electron dynamics to the spatial dimension along the magnetic field lines which greatly improves the stability of the excited Langmuir waves and thus leads to strong and stable electrostatic wiggler fields (Pelletier et al. 1988). For the temperature of both the

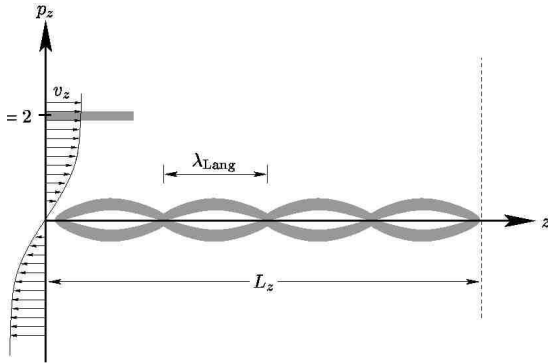


**Fig. 1.** The initial configuration of electron phase space including the beam. The initial disturbance of the background plasma is heavily exaggerated for reasons of better display.

beam- and background electrons values we take the value of  $T_e = T_b = 100$  eV, typical polar cap temperature of neutron stars derived from their thermal X-ray-emission (Pavlov and Petekhin 1995). The PIC-code used for this numerical simulation is fully three dimensional and it conserves mass and energy. In the simulation the direction of electron beam propagation  $\gamma\beta$  and of the magnetic field  $\mathbf{B}$  is the positive  $z$ -direction, which is also called the longitudinal direction. The simulated box has a numerical extension of  $80 \times 80 \times 200$  grid points and a physical extension of  $100 \text{ m} \times 100 \text{ m} \times 250 \text{ m}$ , which corresponds to the size of the expected features. The resolution of  $\delta x = \delta y = \delta z = 1.25 \text{ m}$  is more than sufficient to resolve the expected maximum wavelengths of approximately  $\lambda_{\text{Rad}} = 2\pi/k_{\text{Rad}} = 2\pi c/\gamma^2\omega_{pe} \approx 6.7 \text{ m}$ . A particle density of  $10^{12} \text{ m}^{-3}$  is approximated by 10 quasi particles per cell, leading to 16 million background quasi electrons that are accompanied by a varying number of beam quasi electrons of not more than 2.5 million, which eventually enter the computational box. Those numbers are doubled, since for quasi neutrality an equally large number of positive particles are required.

The initial condition is given by a homogeneous background plasma of density  $n_e$ , temperature  $T_e$  and a longitudinal magnetic field  $B_z = 0.1 \text{ T}$ . This value is found to be sufficiently high to represent a much stronger field of 1000 T. Initially there is no beam in the computational box. The beam is injected later at the  $z = 0$  plane of the box with a density profile of  $n(r) = n_b / (1 + \exp[\frac{r-R}{\Delta R}])$ . Here  $r$  denotes the distance from the  $x$ - $y$  center of the box and  $R = 20 \text{ m}$  and  $\Delta R = 3 \text{ m}$  give the radius and the sharpness of the electron beam. The homogeneous background plasma is disturbed in phase space (see Fig. 1) in order to accelerate the excitation of Langmuir waves by giving the system a hint of the relevant length scales. We used the wave length of the fastest growing Langmuir mode, which follows from an analytic calculation of the linear growth rate. The disturbance is chosen not to in-

duce any finite charge or current densities, thus leaving the background plasma initially homogeneous, neutral and current free.

The boundary conditions during the simulation are quite simple. In the transversal directions  $x$  and  $y$  we chose periodic boundaries and in the longitudinal direction  $z$  the box is open, which means that plasma particles and fields can leave the box unaffected. In addition at the lower  $z$  plane ( $z = 0$ ) an electron component is continuously injected with the density profile mentioned above, a mean  $\gamma\beta$  of 2 and the temperature  $T_b$ .

The simulation runs for 600 time steps with  $\delta t = 2.41 \text{ ns}$ . The total time simulated was  $1.44 \mu\text{s}$ , after which the growing nonlinear Langmuir waves saturate and a quasi stationary situation had developed as it is shown in the next section.

### 3. Results

The beam particles entering the computational box interact with the faint traces of fluctuations we introduced in our initial setup and excite the appropriate modes to grow. In Fig. 6 on page 5 the temporal evolution of the electrons phase space in  $z$ -direction is presented by showing phase diagrams for the time steps 150, 300, 325 and 400. In the first plot (upper left) the penetrating electron beam can be seen together with the background plasma, both are still nearly undisturbed. In the following plots the development of strong Langmuir waves can be observed. After 781 ns, the disturbance in the beam and the background has grown so strong, that both components start to mix, i.e. there is no distinction between beam and background electrons anymore. Beam electrons are strongly decelerated even until  $v \simeq 0$ , whereas background electrons are accelerated up to a Lorenz factor of 5. This can be seen best in Fig. 7 on page 5, where each of the both components are plotted in separate diagrams for the time step 400. In Fig. 7 left the phase space of the beam electrons is shown. Clearly visible are the ring structures of fully developed Langmuir waves. Some of beam electrons are accelerated up to a  $\gamma\beta$  of 4–5 as it is the case for the background electrons, which is shown in Fig. 7 right. On the other hand the beam electrons are also decelerated to zero momentum during their interaction with the Langmuir waves. The extremely strong accelerations are due to the strong electrostatic fields of the excited Langmuir waves. Since the Langmuir turbulence structure in Fig. 6 moves with a much lower speed (which is even continuously decreasing throughout the simulation) than the yet unaffected beam electrons, it acts as the wiggler field that stimulates the CI CS-emission. The electrostatic fluctuations directly correspond to electron density fluctuations (solid curve in Fig. 6), which reach a value of  $\sim +100\% / -50\%$  oriented at  $n = n_e + n_b = 2 \cdot 10^{12} \text{ m}^{-3}$ . The structure of the electron density is better seen in Fig. 8 (page 6) and Fig. 9 (page 7), where the temporal evolution of contour

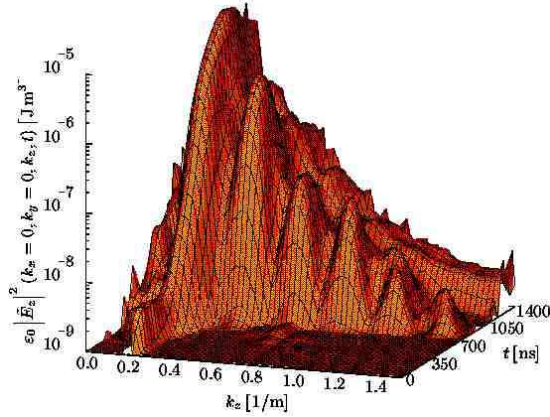


**Fig. 2.** The electrostatic mode energy density is plotted against wavenumber  $k$  and time  $t$ .

surfaces at  $n = 1.5 \cdot 10^{12} \text{ m}^{-3}$  and  $n_e = 1.9 \cdot 10^{12} \text{ m}^{-3}$  and of a cut through the electron beam is shown. The electron density varies between 4 and 1 times  $10^{12} \text{ m}^{-3}$ , which implies the strong electrostatic fields. It can be clearly seen, that the beam decays in a series of "pancakes". Such pancakes are absolutely necessary to explain the coherent nature of the pulsed radio emission of neutron stars. Why? Since the emission from relativistic particles is confined to a forward cone with half angle  $\sim 1/\gamma$  and the emission is nearly along the magnetic field. Thus, in Fourier space bunching emission corresponds to the component  $k_\perp$  to the fields being smaller than the component  $k_\parallel$  along the field line by a factor  $1/\gamma$ . This corresponds to flat pancake shaped bunch with the normal within an angle  $1/\gamma$  of  $B$  (Melrose 2000). This is exactly what we observe in our simulations! We briefly note that our simulations are the first ones which show this kind of pancake bunches! The number of particles in such a pancake corresponds to the the maximum coherence achievable for CICS and it should be noted, that in our simulation the thickness of such a pancake is significantly larger ( $\gtrsim 1 \text{ m}$ ) than the Debye length which is usually used in analytical models. A typical volume of one bunch is about  $10 \text{ m}^3$  giving a total number of particles per bunch of about  $10^{13}$ . Our simulations prove, that a much higher coherence is achievable than expected from analytical models.

The growth of Langmuir waves can be deduced by the Fourier transform of the electrostatic field  $\vec{E}_z$ . In Fig. 2 the energy density of the electrostatic modes is plotted versus the corresponding wavenumber  $k$  and time  $t$ . The  $k \simeq 0.25 \text{ m}^{-1}$  mode is growing by four orders of magnitudes within some ten nanoseconds. It should be noted however, that the fastest growing mode is slightly off compared to the initially given wave number can be seen in Fig. 2 as the small peak at early times. This means, that for our simulation the analytical value for the fastest growing mode is not precisely correct and it proves, that although the initial disturbance has given a hint to the system it has

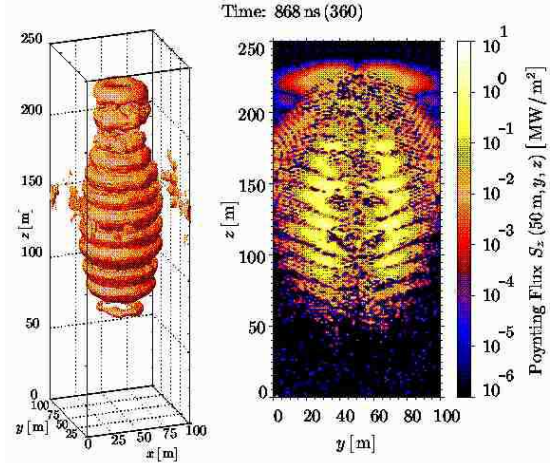


**Fig. 3.** Structure of the emitted pointing flux as 3D contour surface of the value  $2.5 \cdot 10^4 \text{ W/m}^2$  (left) and as a cut through the center of the beam at  $x = 50 \text{ m}$  (right).

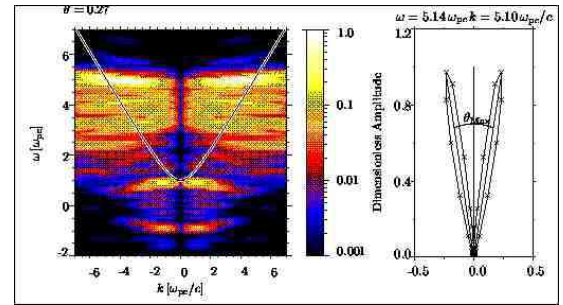


**Fig. 4.** Dispersion relation (left) and emission characteristic (right) of the emitted radiation. For the left plot the angle  $\theta_M$ , the angle of maximum intensity, has been used. The curve in the left plot gives the dispersion branch of electromagnetic radiation in a plasma. The right diagram presents the intensity of the radiation for a given  $\theta$  in a polar plot.  $\theta$  is the angle between beam direction and direction of emission. The values in both diagrams are normalized to a value of one.

not forced it towards an unphysical solution. We note that the wave energy density is distributed to higher  $k$  when it exceeds a value of about  $10^{-7} \text{ J m}^{-3}$ , driven by nonlinear wave-wave interactions.

It is important to recognize that the generated electrostatic fluctuations react on the beam electrons similar to the wiggler fields in the laboratory FEL, with one major difference. In our case the wave wiggling self-consistently excited is along the propagation direction of the beam, whereas in the FEL-case the external magnetic wiggling is perpendicular to the beam propagation. The strongest emission originates in regions with the largest density gradients Fig. 3. Every de- and acceleration region forces the beam electrons to emit Hertz' dipole radiation, which is beamed in forward direction, as can be seen in Fig. 4 (right).  $\theta_M$  represents the angle

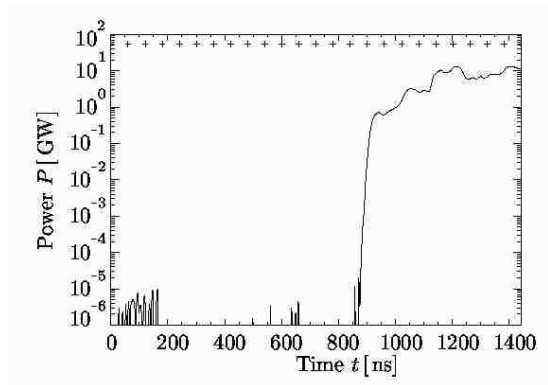


**Fig. 5.** Total integrated poynting flux leaving the computational box at the top ( $z = 250$  m) against time. The + symbols show the total power injected as kinetic energy of the beam electrons.

of maximum intensity, expected from theoretical consideration ( $\tan \theta_M = 1/2\gamma\beta$ ) with a  $\gamma\beta = 2$ . The striking resemblance with a relativistically beamed Hertz' dipole is obvious, but the emission characteristic in our simulation also gives precisely the expected opening angle of the emission cone, which is proposed for a CICS-process. In Fig. 4 (left) the "spectrum" of the emitted radiation is shown, which has a strong peak at  $\omega = 5\omega_{pe}$  and a couple of minor peaks at  $4\omega_{pe}$  and  $3\omega_{pe}$  due to nonlinear wave coupling. Again we find rather precisely the theoretically expected value of  $w = \gamma^2\omega_{pe}$ . The total power emitted by the simulated computational box is shown in Fig. 5. It is the escaping poynting flux at the top of the computational box ( $z = 250$  m) integrated over the top surface. After about 850 ns the emitted power rises within some ten nanoseconds by more than 6 orders of magnitude to a value of 1 GW. Afterwards the total output power increases more slowly by one more order of magnitude and reaches a maximum of 10 GW continuous radiative power at the end of the simulation. This is a significant fraction of the power injected by kinetic energy of the beam particles, shown in Fig. 5 as + symbols at a constant value of 50 GW. The rest of the energy leaves the box as kinetic energy of beam electrons, which would probably be also emitted if the computational would have a greater size in  $z$ -direction.

#### 4. Discussion

We have shown that in a strongly magnetized plasma a relativistic electron beam can be forced to emit highly coherent radio emission by self-induced nonlinear density fluctuations. Such slowly moving nonlinear structures oscillate with the local plasma frequency at which the relativistic electrons are scattered. Beam electrons dissipate a significant amount of their kinetic energy by inverse Compton radiation at a frequency of about  $\gamma^2\omega_{pe}$ . Since the beam is sliced into pancake structures which experience the same

electric field the inverse Compton scattering is coherent. Such a process is a very promising candidate for the coherent radio emission of pulsars.

#### Acknowledgments

*Acknowledgements.* The authors would like to thank the John von Neumann Institute for Computing (NIC) and the Leibniz Rechenzentrum München for the granted computational time and the Deutsche Forschungsgemeinschaft which supported our work through the grant LE 1039/3-1.

#### References

- Benford, G., Weatherall, J.C., 1991, ApJ, 378, 543
- Kato, K., Benford, G., Tzsch, D., 1983, Phys. Fluids, 26, 3636
- Kunzl, T., Lesch, H., Jessner, A., von Hoensbroch, A., 1998, ApJ, 505, L139
- Levron, P., Benford, G., Tach, D., 1987, PRL, 58, 1336
- Melrose, D.B., 2000, in Pulsar Astronomy IAU Colloq. 177, ASP. Conf. Series 202, 721
- Melrose, D.B., Gedalin, M., 1999, ApJ, 521, 351
- O'Shea, P.G., Freund, H.P., 2001, Science, 292, 1853
- Pavlov, G.G., Petekhin, A.Y., 1995, ApJ, 450, 883
- Pelletier, G., Sol, H., Asseo, E. 1988, Phys. Rev. A, 38, 2552
- Rickett, B.J., 1995, ApJ, 197, 185
- Weatherall, J.C., 1988, PRL, 60, 1302



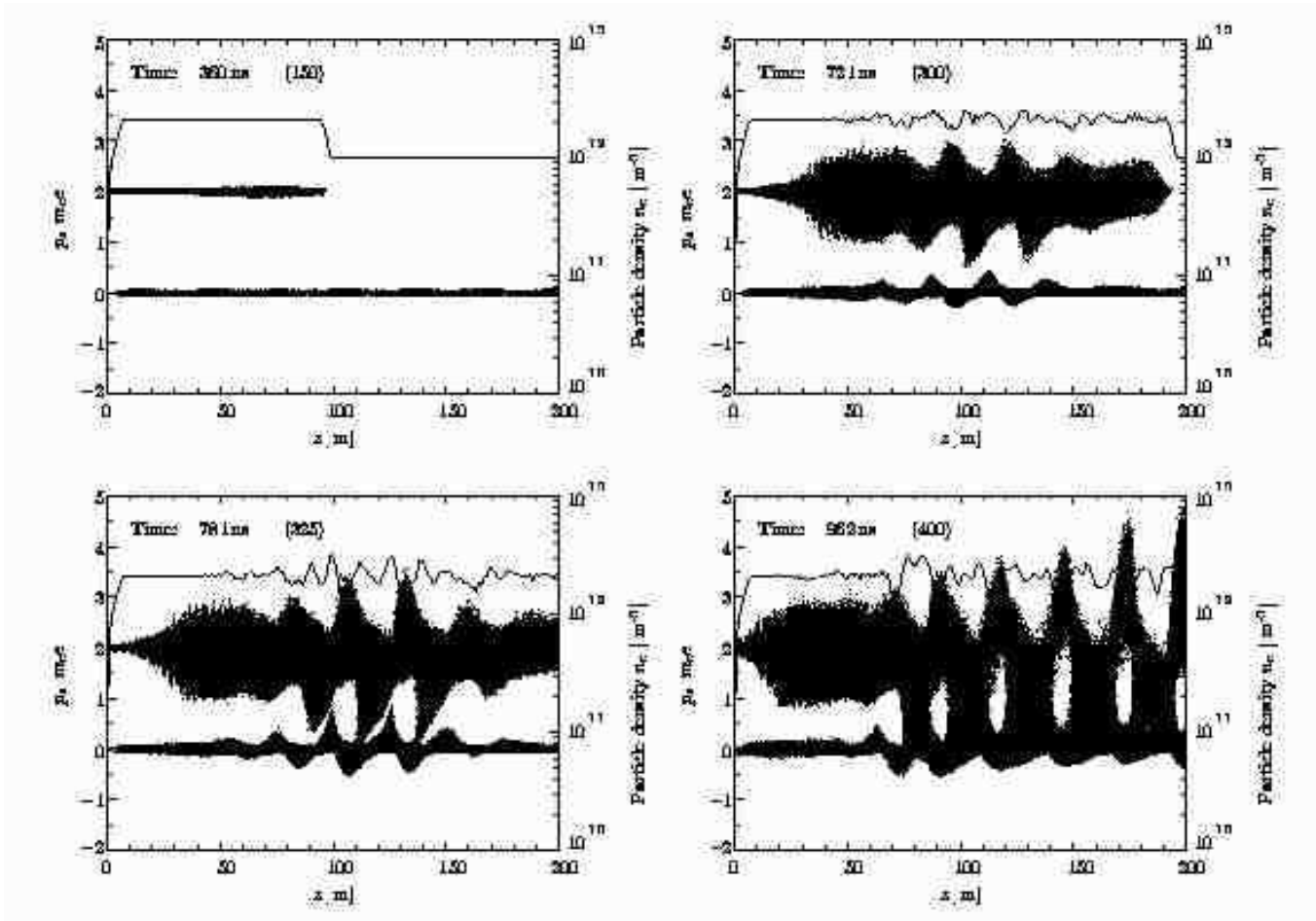


**Fig. 6.** Electron phase space in  $z$ -direction after 150, 300, 325 and 400 timesteps. The quasi particles are plotted as dots according to their corresponding position in  $z$  (ordinate) and their momentum  $p_z$  (left abscissa). The solid curves present the particle density of the electrons (right abscissa).

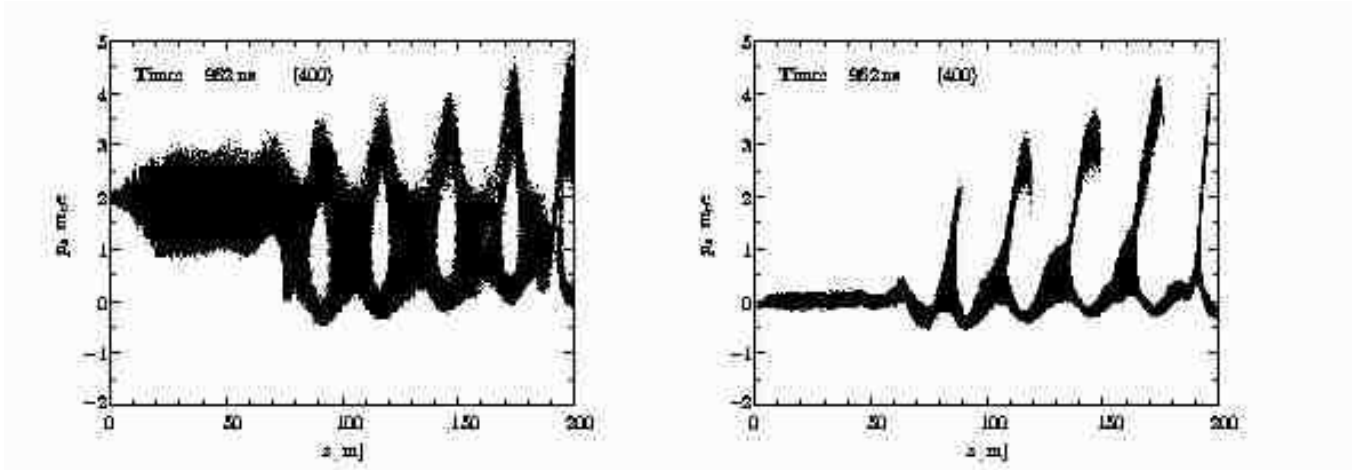


**Fig. 7.** Electron phase space in  $z$ -direction after 400 timesteps separated for beam (left) and background (right) electrons.

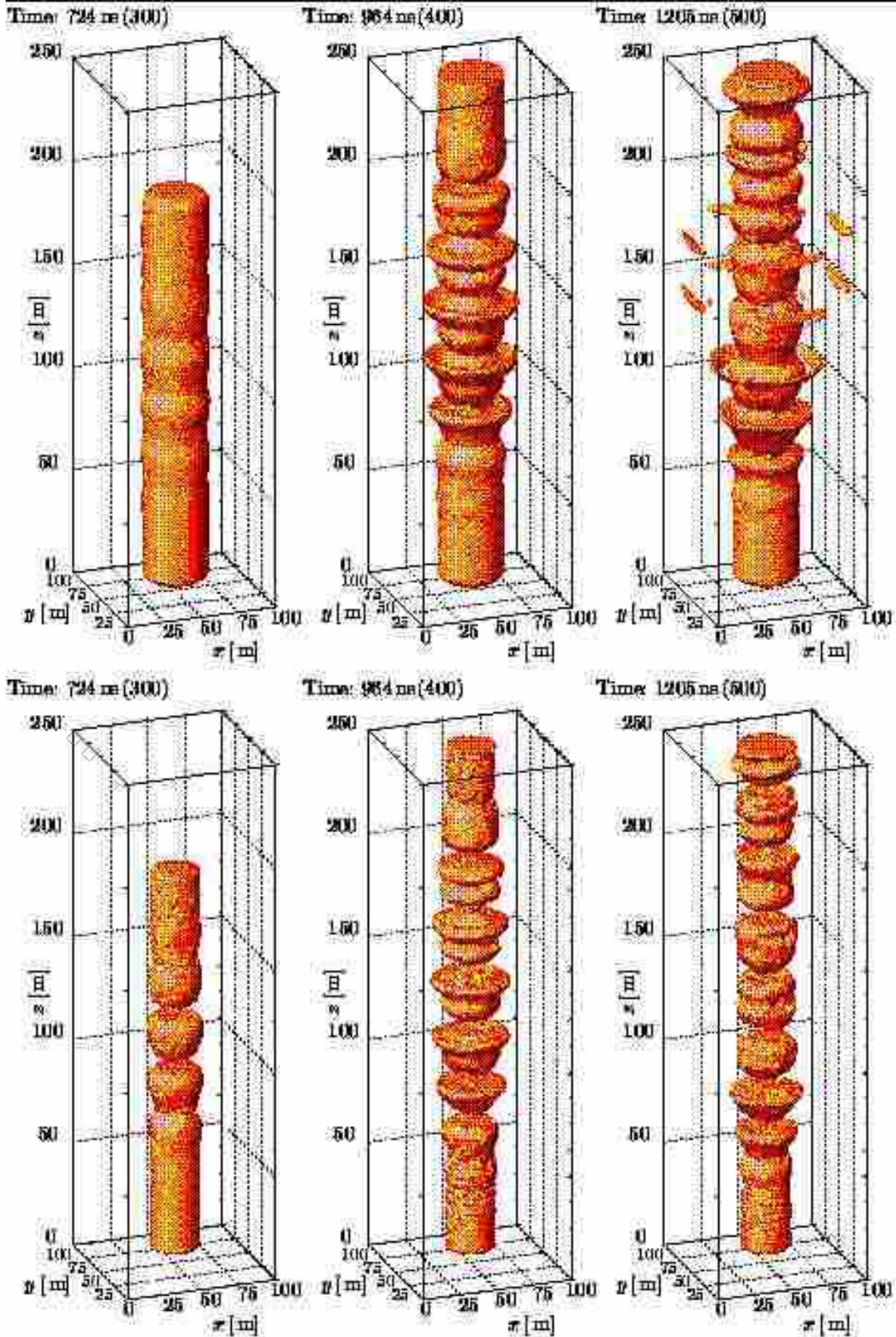


Fig. 8. Three dimensional contour plots of the electron particle density. For the timesteps 300, 400 and 500 (left to right) the surfaces are shown, where the density is  $n = 1.5 \cdot 10^{12} \text{ m}^{-3}$  (top) and  $n_e = 1.9 \cdot 10^{12} \text{ m}^{-3}$  (bottom) respectively.



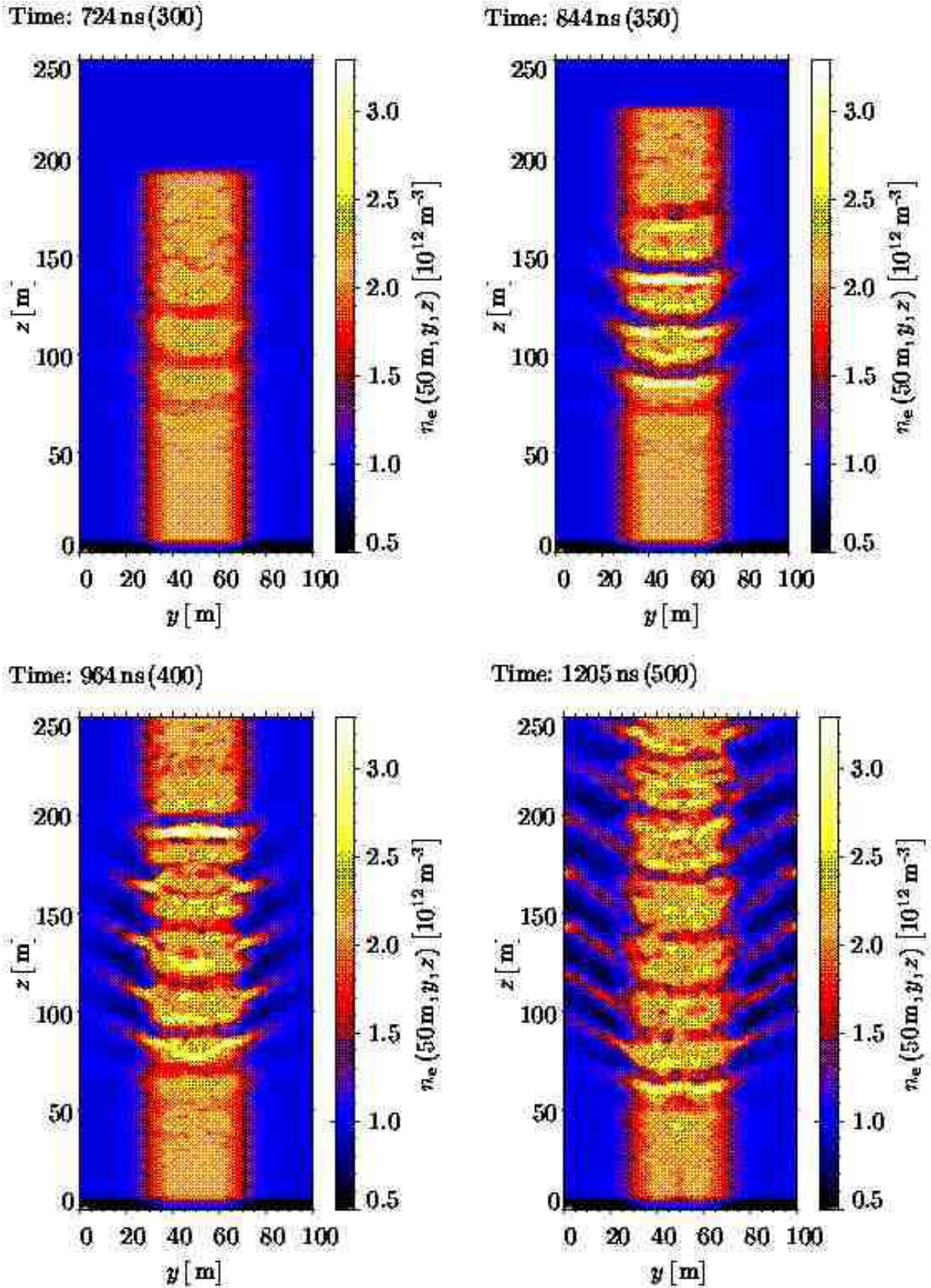


Fig. 9. two dimensional contour plots of the electron particle density at timesteps 300,350,400 and 500. Shown is a cut through the center of the penetrating electron beam at  $x = 50 \text{ m}$ .